Composites: Part A 162 (2022) 107168

Contents lists available at ScienceDirect

Composites Part A

journal homepage: www.elsevier.com/locate/compositesa

Experimental characterisation of large in-plane shear behaviour of unidirectional carbon fibre/epoxy prepreg tapes for continuous tow shearing (CTS) process

Bohao Zhang, Byung Chul Kim *

Bristol Composites Institute (ACCIS), University of Bristol, Queen's Building, University Walk, Bristol BS8 1TR, United Kingdom

ARTICLE INFO

Keywords:
Carbon fibre
Mechanical testing
Automated fibre placement
High-temperature properties
Defects

ABSTRACT

The continuous tow shearing (CTS) process is an advanced tape placement technique with the ability to steer unidirectional prepreg tapes by in-plane shear deformation without the presence of tape buckling, gaps and overlaps. However, the inherent fibre misalignment within the tape can induce fibre waviness during the shearing process, which is further affected by processing parameters such as temperature, shear rate and fibre tension. In this paper, the effect of those parameters on the shear behaviour of two different unidirectional carbon/epoxy prepreg tapes was experimentally investigated. A bespoke test fixture was designed to shear the tape specimens at various shear rates and fibre tensions. Digital image correlation (DIC) was used to obtain full-field strains of the specimens to investigate the fibre realignment during shearing. Experimental results showed that both temperature and fibre tension significantly affect the uniformity of the fibre realignment. Moreover, the responses of the two prepreg tapes under the same shearing condition were different due to their different impregnation characteristics.

1. Introduction

1.1. Continuous tow shearing process

Automated fibre placement (AFP) and automated tape laying (ATL) processes have been widely used to automatically lay down unidirectional (UD) carbon fibre/epoxy prepregs tapes onto moulds following pre-defined placement paths for large-scale composite parts, such as airplane fuselage, wing skins and automotive components [1]. However, defects such as tape overlaps and gaps between adjacent tapes [2], out-of-plane wrinkling/buckling, and fibre waviness/misalignment [3] form when steering prepreg tapes along a circular path with a small steering radius [4]. Such defects have been a challenging issue in design and manufacture of fibre-steered composite structures. In order to solve the problem of the fibre-steering-induced defects, Continuous Tow Shearing (CTS) process has been developed at the University of Bristol [5]. In this process, a UD prepreg tape is heated and continuously sheared (rather than bent) in plane, while realigning the fibres along the pre-defined steering direction. It has been experimentally demonstrated that a prepreg tape can be steered at a minimum steering radius, which is an order of magnitude less than that of the current AFP machines, without the presence of any macroscopic defects regardless of the tape width [5–7]. In the recent investigation, it was found that the microscopic scale fibre waviness could be generated in the CTS process, which may be attributed to the processing parameters as well as the inherent fibre misalignment within the prepreg tape material [7].

Fig. 1 shows the working mechanism of the CTS process. One end of the prepreg tape (with the backing paper) is gripped by the pinch device, which comprises the tape guide roller and the gripping shoe, while the other end of the tape is compressed onto the mould by the compaction shoe. The backing paper is pulled and separated at the front end of the gripping shoe. The prepreg tape is heated prior to be fed into the pinch device, and kept warm until it is sheared. The head moves along the shifting direction (i.e. tape width direction) as well as the opposite direction to the tape feeding direction to allow the compaction shoe slides on the tape already laid, therefore achieving continuous in-plane shear deformation of the tape within the shearing gap. During the shearing, the fibres of the prepreg tape within the shearing gap are re-aligned along the moving direction of the head without buckling. The tension applied to the prepreg tape within the shearing gap is determined by the resistance force required to pull out the prepreg tape from the material dispensing unit and the tension force applied to the backing paper.

* Corresponding author.
E-mail address: B.C.Eric.Kim@bristol.ac.uk (B.C. Kim).

https://doi.org/10.1016/j.compositesa.2022.107168
Received 6 May 2022; Received in revised form 16 August 2022; Accepted 19 August 2022
Available online 24 August 2022

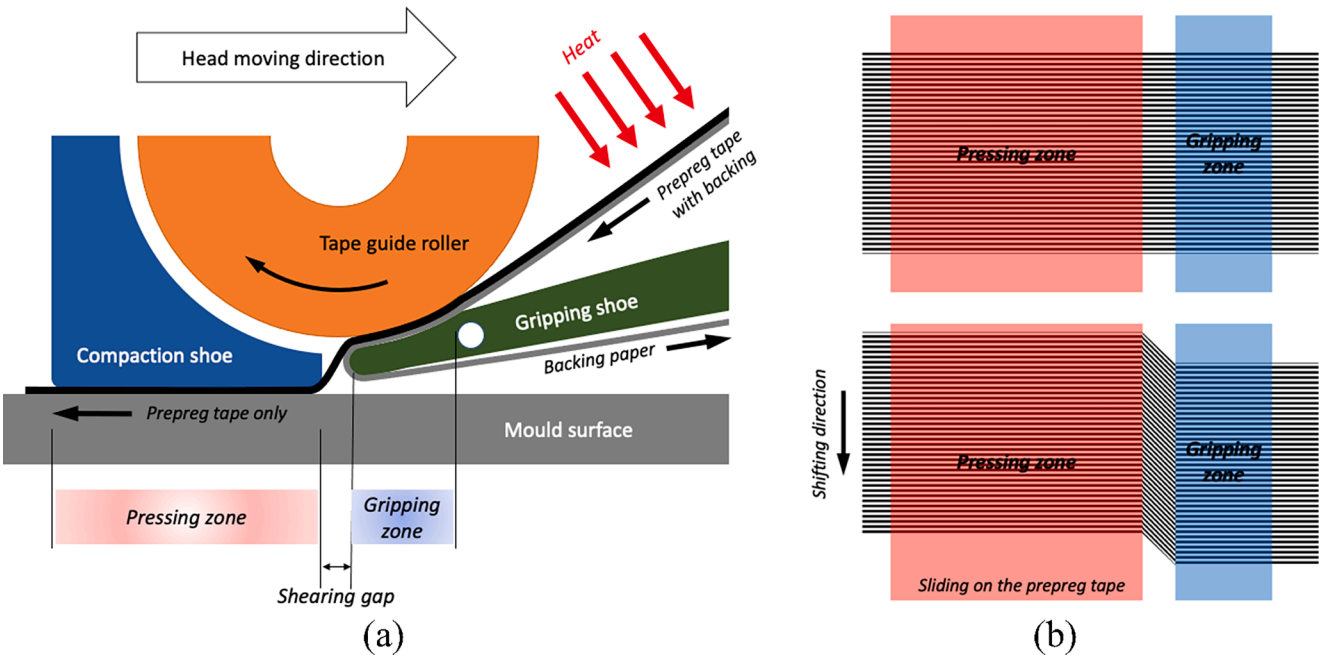

Fig. 1. The continuous tow shearing (CTS) mechanism: (a) schematic (side view), (b) top view of the relative movement of the pressing zone (compressed by the compaction shoe) and gripping zones (compressed by tape guide roller and gripping shoe). Reproduced from Ref. [5].

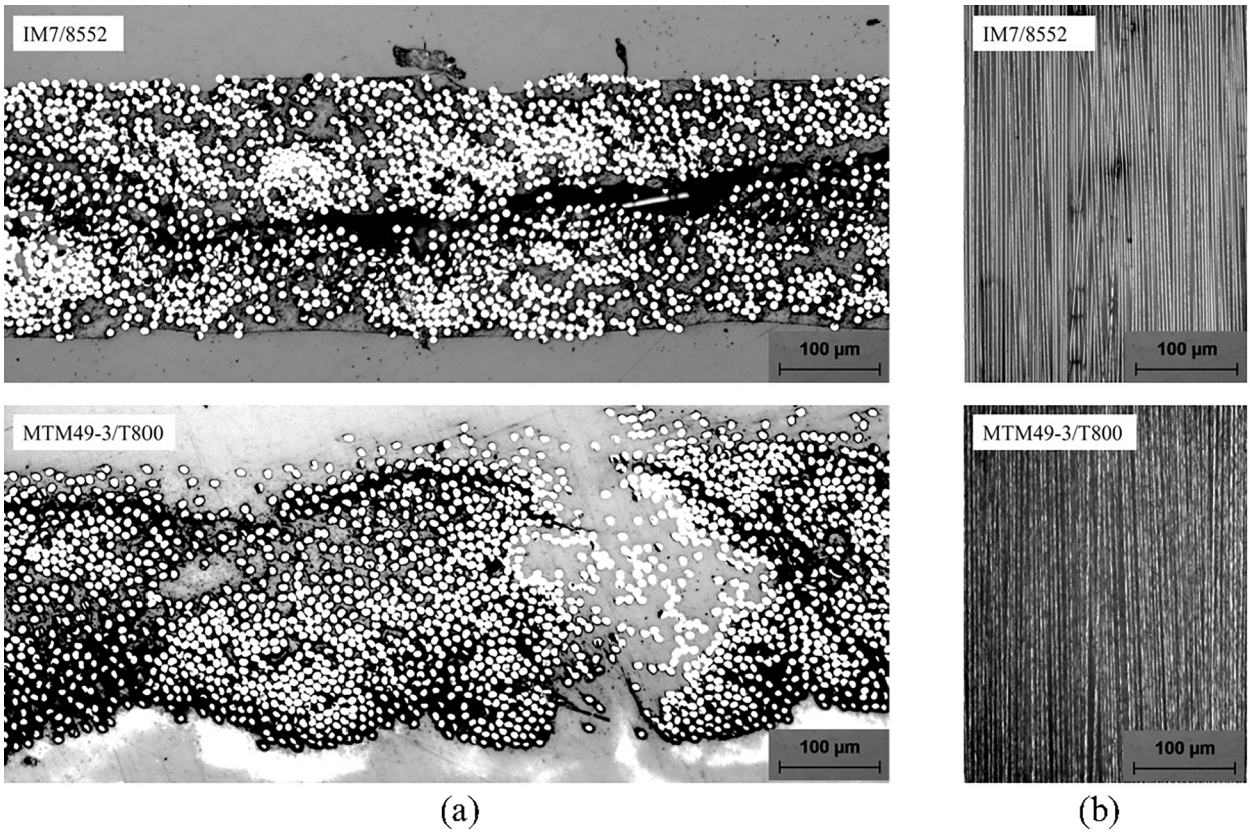

Fig. 2. Microscope images of: (a) the cross sections and (b) the surfaces of IM7/8552 (top) and MTM49-3/T800 (bottom) prepregs.

Although this novel mechanism allows for eliminating fibre-steering induced defects, the previous layup test results have shown that the prepreg material type and the processing conditions affected the quality of fibre realignment [6,7]. It is important to understand these effects through material characterisation tests for the optimisation of the CTS process without conducting costly and time-consuming layup tests.

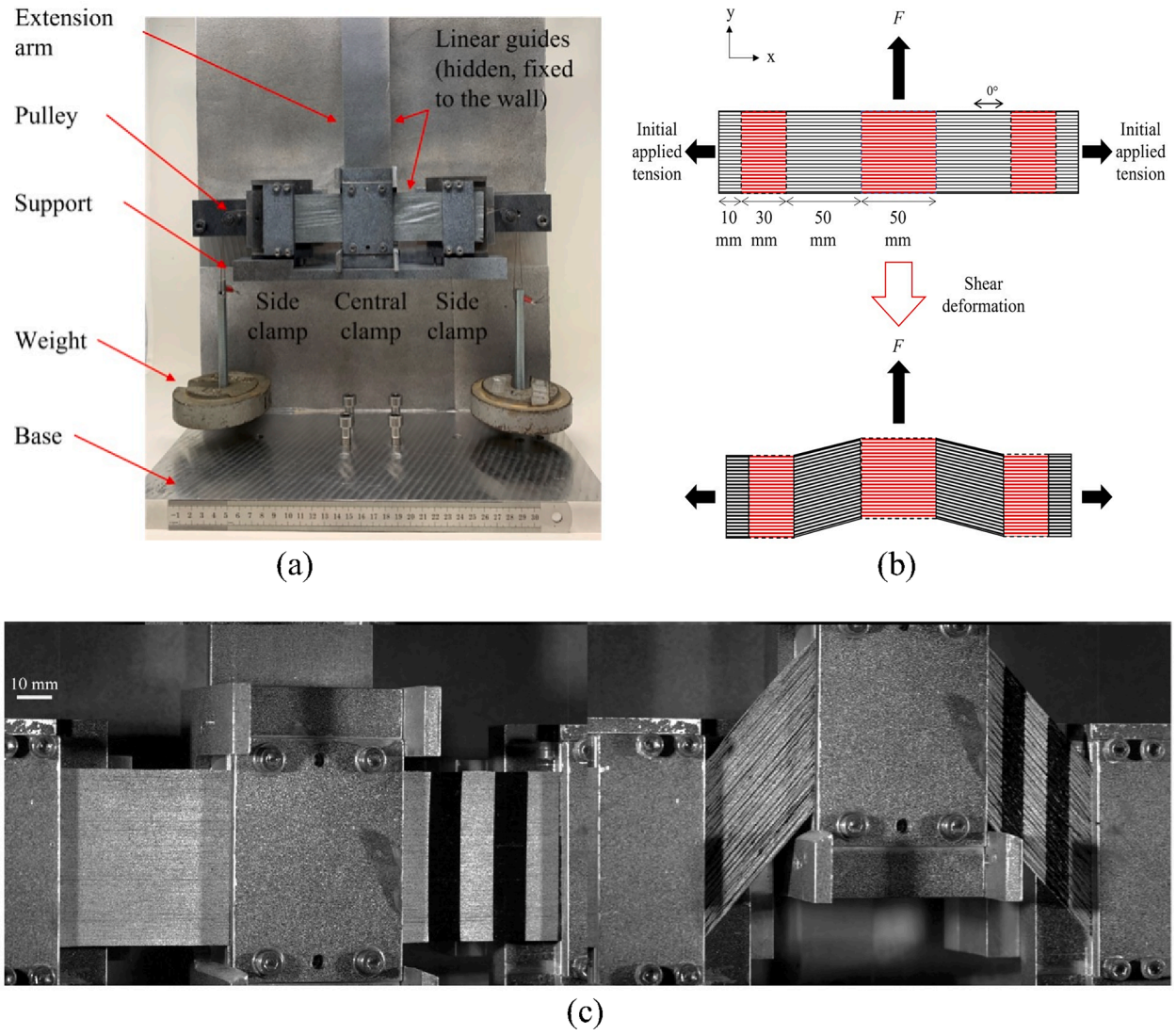

Fig. 3. (a) The bespoke in-plane shear test fixture, (b) schematics of the shear deformation and (c) photos of the specimen before and after shear deformation at 0° shear angle (left) and 46° shear angle (right).

1.2. Characterisation of the shear behaviour of carbon fibre/epoxy prepreg tapes

It is important to understand the in-plane shear behaviour of UD prepreg tapes in order to optimise the CTS process. The two test methods commonly used to characterise the in-plane shear deformation of composite reinforcements are the picture frame and bias extension tests [8,9]. However, these methods are limitedly used for woven fabric reinforcements in the ±45° configuration [8–11], as fibres are required in both directions to achieve a force equilibrium within the test fixture.

There were a few attempts to use those methods for UD prepreg materials. McGuinness and ÓBrádaigh [12] attempted the picture frame test on cross-plied specimens of a UD carbon/PEEK prepreg material and investigated the effect of temperature and shear rate on the shear force and viscosity response of the material. Potter [13] carried out bias-extension tests of cross-plied UD prepreg tapes and reported fibre wrinkle formation due to the fibre misalignment and formation of shear bands in the specimens tested at high deformation speeds. Larberg et al. [14] performed the bias extension test on cross-plied UD carbon/epoxy prepreg tapes, and showed that the shear behaviour was influenced by the crosshead speed and the shear stiffness of the materials decreased with increasing testing temperature. However, most of the previous studies were for cross-plied UD carbon prepregs, which could behave differently from pure UD prepregs. Recently, Wang et al. [15] conducted 10° off-axis tensile tests of UD carbon/epoxy prepreg tapes. However, the maximum shear strain achieved was only 8% (5° in degrees), which was much smaller than the shear angle range used in the CTS process. Also, transverse tensile stress applied to the shear band might cause transverse spreading, making the deformation different from pure shear.

1.3. Research aim

The aim of this study is to investigate the effect of the CTS processing conditions on the in-plane shear behaviour of UD carbon/epoxy prepreg tapes via a unique in-plane shear test method. This method can be used to optimise the CTS process conditions without conducting time-consuming and costly lay-up trials. A bespoke test fixture was designed to achieve pure shear deformation of UD tape specimens subjected to the actual CTS processing conditions. The effects of processing temperature, shear rate and applied fibre tension on the fibre realignment and shear stiffness during shearing were experimentally investigated by measuring full-field displacement and strain of the sheared specimens.

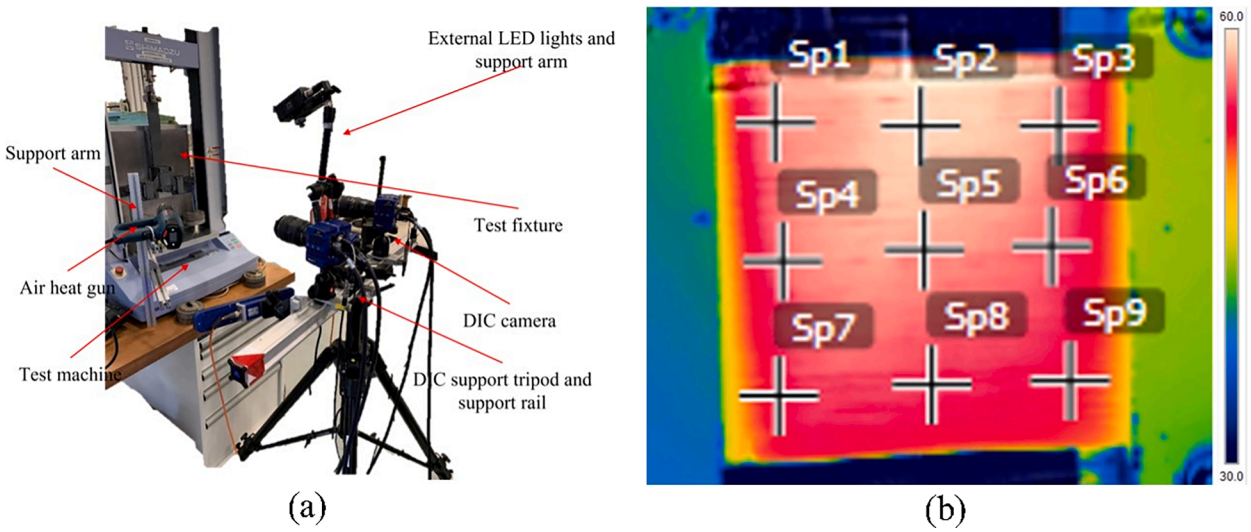

Fig. 4. (a) The test setup and (b) the specimen surface captured by an infra-red camera. (For interpretation of the references to colour in this figure legend, the reader is referred to the web version of this article.)

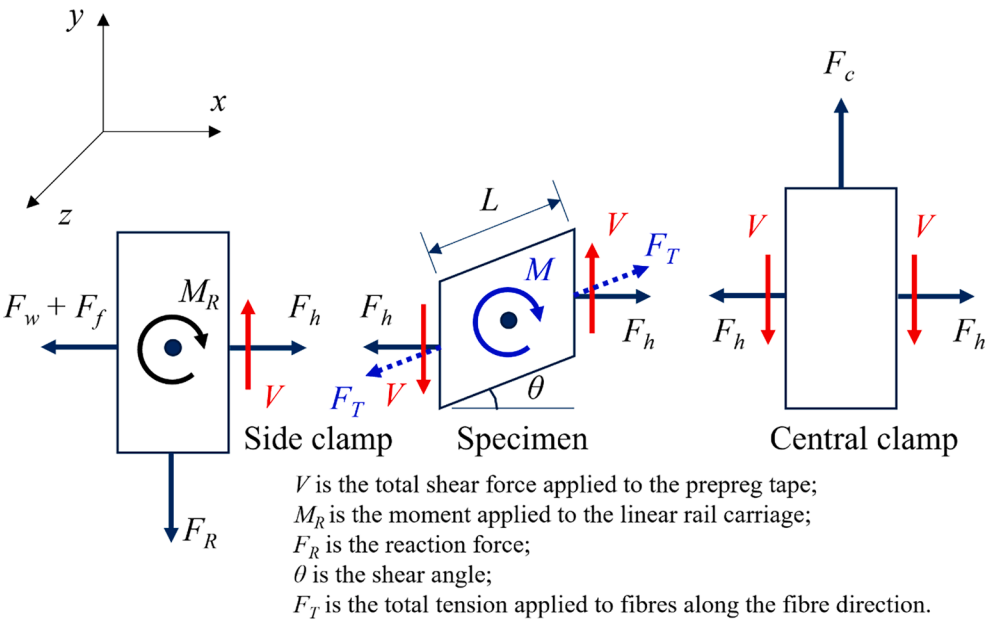

Fig. 5. The free body diagram of the specimens subjected to shear deformation (only one side of the specimen is sketched due to the symmetry).

2. Experimental investigation

2.1. Materials

Two UD carbon/epoxy prepregs (HexPly IM7/8552, Hexcel, UK and Solvay MTM49-3/T800, Solvay, UK) were used. Both prepregs are made of 12 K never twist grade fibre tows. The fibre areal weight and the cured ply thickness of IM7/8552 were 130 g/m^2 and 0.125 mm and of MTM49-3/T800 were 140 g/m^2 and 0.14 mm. The elastic moduli of the IM7 and T800 fibres are 276 GPa and 294 GPa, respectively. The viscosities of the resin matrices of both prepregs are similar in the temperature range of 25–70 °C [16]; approximately 22,000 PaS at 25 °C, 1400 PaS at 50 °C, 220 PaS at 70 °C. However, they showed different impregnation characteristics. Fig. 2 shows the cross sections and surfaces of both prepreg specimens cured at 35 °C for a long period and potted in epoxy. For the IM7/8552, fibres were well distributed and impregnated with the resin, but large voids were distributed horizontally at the middle of the ply. In comparison, for the MTM49-3/T800, large resin-rich areas were observed with voids distributed more randomly. Examination from surface images revealed that the IM7/8552 prepreg exhibited greater fibre misalignment than the MTM49-3/T800 prepreg in general, despite its worse impregnation quality.

2.2. Test fixture and setup

In order to achieve pure shear deformation of the UD prepreg specimens to a large shear angle, a bespoke test fixture was developed. As shown in Fig. 3(a), it consists of a central clamp on a vertical linear guide rail and two side clamps on horizontal linear guide rails. The rails were mounted on a thick aluminium plate fixed on to the base of a tensile test machine. A 5 mm thick aluminium extension plate was attached to the central clamp to connect it to the crosshead. A metal wire was attached to each side clamp to apply horizontal tensile force to the specimen using weights via a pulley. A 50 mm wide and 230 mm long 0° UD

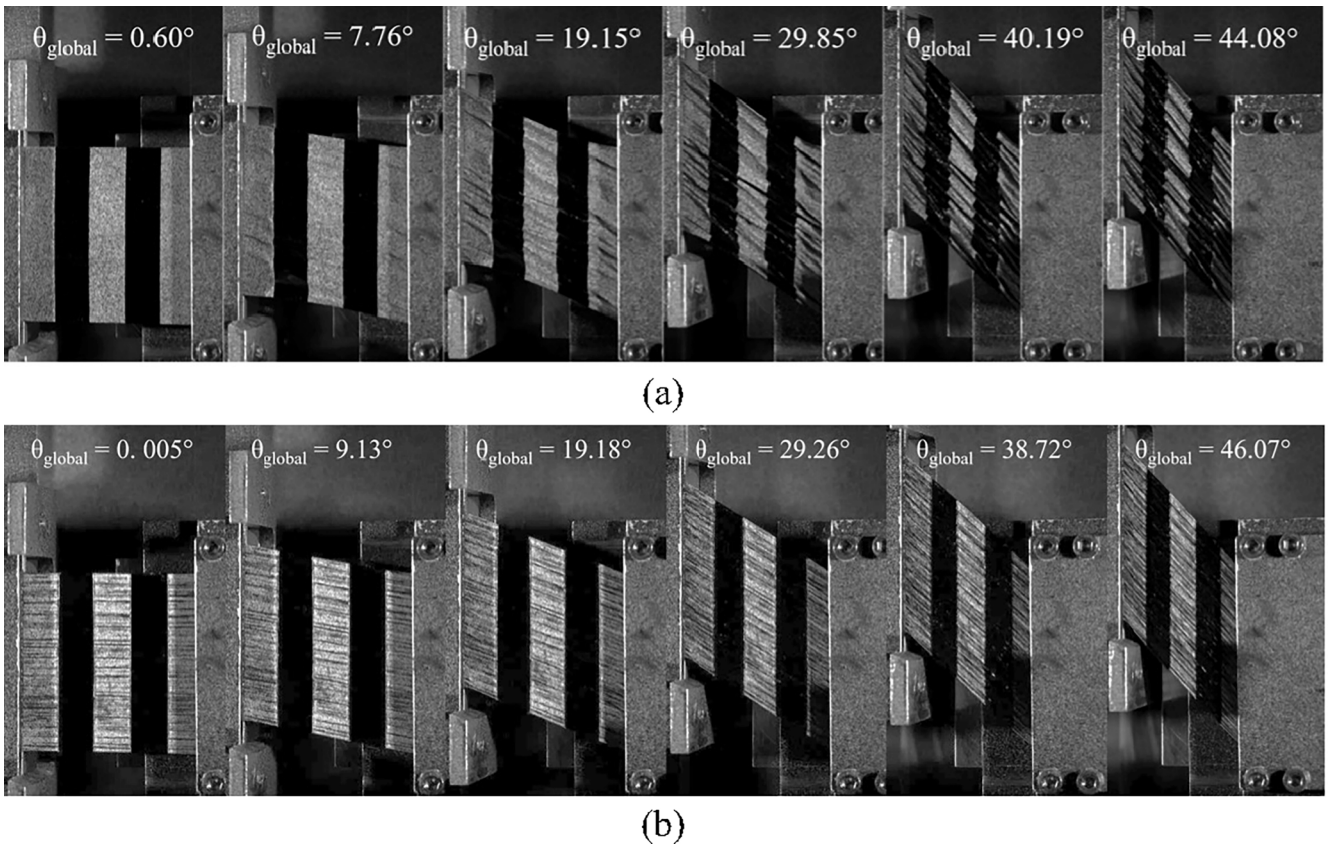

Fig. 6. Continuous photos of the IM7/8552 prepreg specimens sheared at (a) room temperature (RT) and (b) 70 °C (tested at shear rate: 0.01 rad/s, initial applied tension: 0.8 N/mm).

specimen prepared from the as-manufactured prepreg roll was gripped using the clamps with aluminium top plates.

To achieve the intended in-plane shear deformation of the prepreg tape, the central clamp pulled upwards, while the side clamps moved accordingly towards the central clamp (see the schematic in Fig. 3(b)). In this way, the prepreg tape was sheared in the pure shear mode. The maximum achievable shear angle of the test fixture was 55°. To ensure the initial fibre straightness during specimen mounting and the 50 mm long shearing gap (i.e. distance between the central clamp and the side clamp), an aluminium support was attached to the side clamps and removed prior to testing.

The shear tests were conducted in a tension mode with a 1 kN load cell. As shown in Fig. 4(a), two heat guns were attached on the fixture at about 300 mm away from each testing area of the specimen. An infra-red camera (FLIR T650c, FLIR, US) was used to measure the temperature of the specimen. The temperature difference of nine different locations of the specimen surface was about 3 °C (see Fig. 4(b)). To achieve constant shear rates ($\dot{\theta}$), the crosshead speed ($V_{crosshead}$) of the test machine was calculated as below.

$$V_{crosshead}(\delta) = \sqrt{L^2 - \delta^2} \times \dot{\theta} \tag{1}$$

where L is the initial shearing gap of 50 mm and δ is the crosshead displacement. The calculated crosshead speed was then input into the control software of the test machine in a tabular form.

2.3. Full-field displacement measurement

LaVision Stereo DIC system with two 16-megapixel, imager E-lite stereo cameras were used to measure the 3-dimensional full-field displacements in the shearing region of the specimen (as shown in Fig. 4 (a)). Subset size of 31 pixel (in equivalent to 0.52 mm) and step size of 15 pixel (in equivalent to 0.26 mm) were used; The pixel resolution in x, y and z dimensions was 0.017 mm. A high contrast speckle pattern was applied on the surface of each prepreg tape specimen (see Fig. 3(c)). This was done by spraying white speckles on the specimen surface first and then spraying black speckles. Also, a stripe pattern of 10 mm width was created on the right shearing region to observe the tow splitting and inter-tow shearing. The stripe was created by firstly covering the specimen surface with a 10 mm wide masking tape and then applying white and black speckles as described above.

A nodal mesh with elements of the same size as the defined subset size in the sheared region of the specimens was first obtained using the DIC processing software (DAVIS 8). Then, the local shear angle of each element (θ_{local}) was calculated using two spatial vectors of each element. Also, the global shear angle (θ_{global}) was calculated using the measured displacements of the two shearing boundaries for comparison. Also, the surface roughness of the tested area was obtained by tracking the out-of-plane displacements of the nodes on the centre line of the undeformed same nodal mesh. The root-mean-square deviation (R_q) and total number of peaks (R_{Pc}) were then calculated from each surface profile.

2.4. Test conditions

In the CTS process [5], the shear rate ($\dot{\theta}$) is associated with the steering radius and laying speed and is given by

$$\dot{\theta} = \frac{d\theta}{dt} = \frac{V}{R} \tag{2}$$

where t is time, V is the lay-up speed and R is the steering radius. It has been reported that the minimum steering radius could be 50 mm at the steering speed of 5 mm/s [6], which corresponds to the shear rate of 0.1 rad/s. As the steering radius decreases, the shear rate is increased. In this

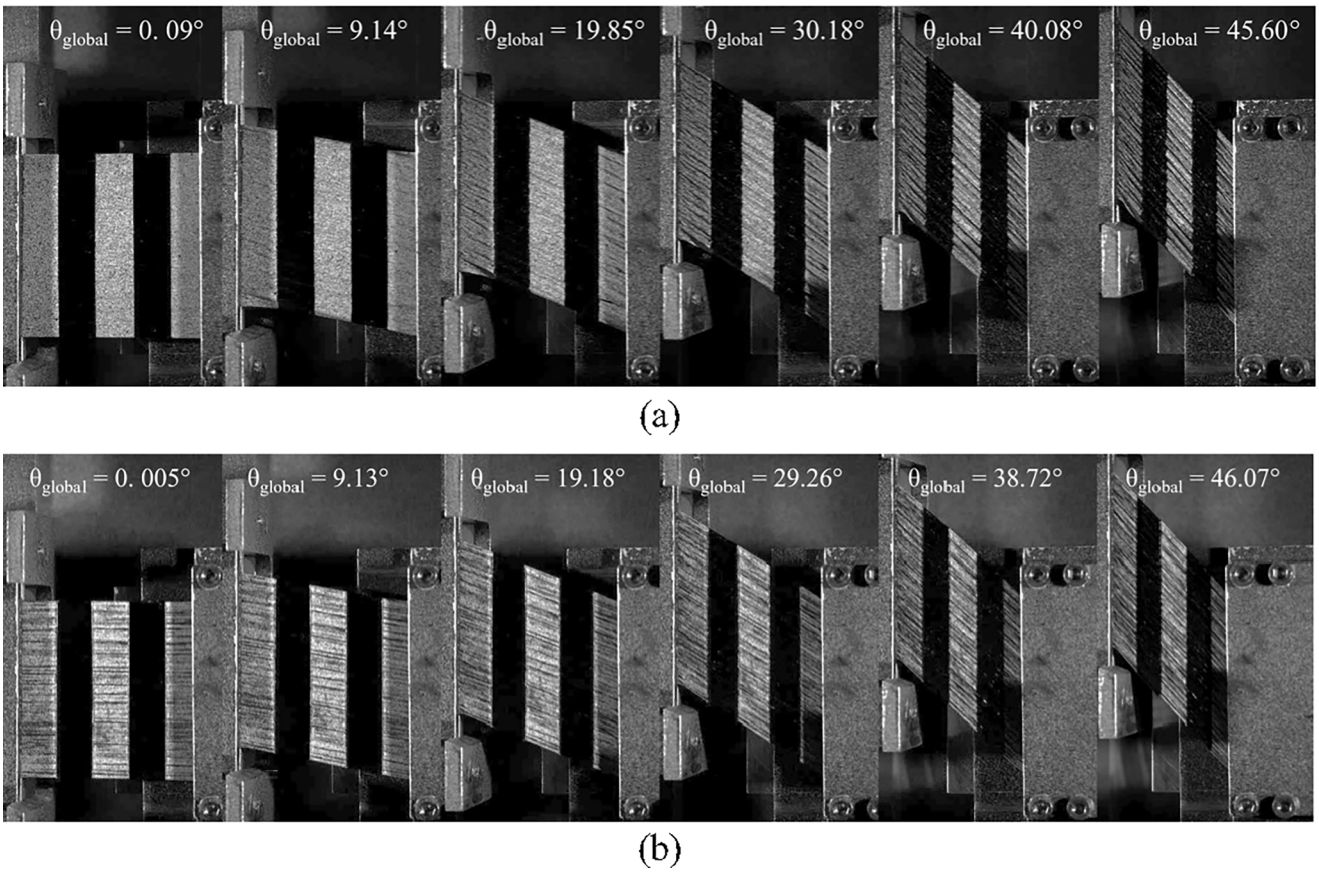

Fig. 7. Continuous photos of the MTM49/T800 prepreg specimens sheared at (a) room temperature (RT) and (b) 70 °C (shear rate: 0.01 rad/s, initial applied tension: 0.8 N/mm).

work, the shear rates of 0.01, 0.1 and 0.3 rad/s were used. The specimens were tested at room temperature, 50 °C and 70 °C in which the viscosity of both prepreg materials is similar and reduced by a factor of 10 at these temperatures. In addition, the specimens were sheared at the initial applied tension per unit specimen width of 0.2, 0.4, 0.6 and 0.8 N/mm. Three specimens per each test configuration were used.

2.5. Characterisation of the in-plane shear resistance

Fig. 5 shows the free body diagram of one side of a specimen under large shear deformation, assuming that only its global response is of interest. It shows that applied shear force (V) is applied to the two specimen edges, inducing bending moment (M_R) to the side clamp. Internal moment (M) is induced by the viscous matrix resin resisting fibre rearrangement (i.e. inter-fibre friction and shear stress) within the prepreg tape. The tensile force applied to the specimen along the fibre direction (F_T) at a given shear angle (θ) can be calculated by

$$F_T = F_h \times \cos\theta + \frac{1}{2}F_C \times \sin\theta \tag{3}$$

where F_w is the horizontal tensile force applied by the weights, F_f is the friction force on the horizontal linear guide rail, F_h is a summation of F_w and F_f, and F_C is the crosshead force. The friction force was measured from the shear tests with the dry fibre tows in the same configuration as the prepreg specimens at zero applied tension force and at room temperature.

According to the moment equilibrium, the material shear force applied to the specimen (V_m), which balances with the internal moment (M), can be calculated by

$$V_m = V - F_h \times \tan\theta = \frac{1}{2}F_C - F_h \times \tan\theta \tag{4}$$

The shear stress along the clamped boundary cannot be uniform as the specimen has free edges. Therefore, shear force was used rather than shear stress.

3. Results

3.1. General in-plane shear behaviour

Ideally, upon in-plane shear deformation, all individual fibres within the specimen should be rearranged slipping relative to each other and perfectly aligned at the global shear angle developing pure intra-tow shearing (i.e. fibre-level slip within tows) without inter-tow shearing (i.e. slip of tows comprising the prepreg or inter-tow slip); the intra-tow and inter-tow shears have been well described in Ref. [20], and have observed even in the picture frame and bias extension tests of fabric prepregs [9,17]. In this process, since the surface area of the sheared specimen decreases during shearing due to the clamped boundaries of the specimen, the fibres should also be forced to move out of the plane for their rearrangement within the ply.

However, such ideal fibre rearrangement can occur only when the effect of the viscous resin is negligible and the fibre tension level is high. Differently from woven fabric prepregs, out-of-plane fibre movements in a UD prepreg are not well constrained except at the clamped boundary regions. This made a few other mechanisms involved such as global wrinkling and micro wrinkling caused by tow splitting and twisting. Global wrinkling occurred when the out-of-plane fibre movements within each tow were difficult to occur; this is similar to the wrinkling of a membrane material subjected to simple shear due to the transverse

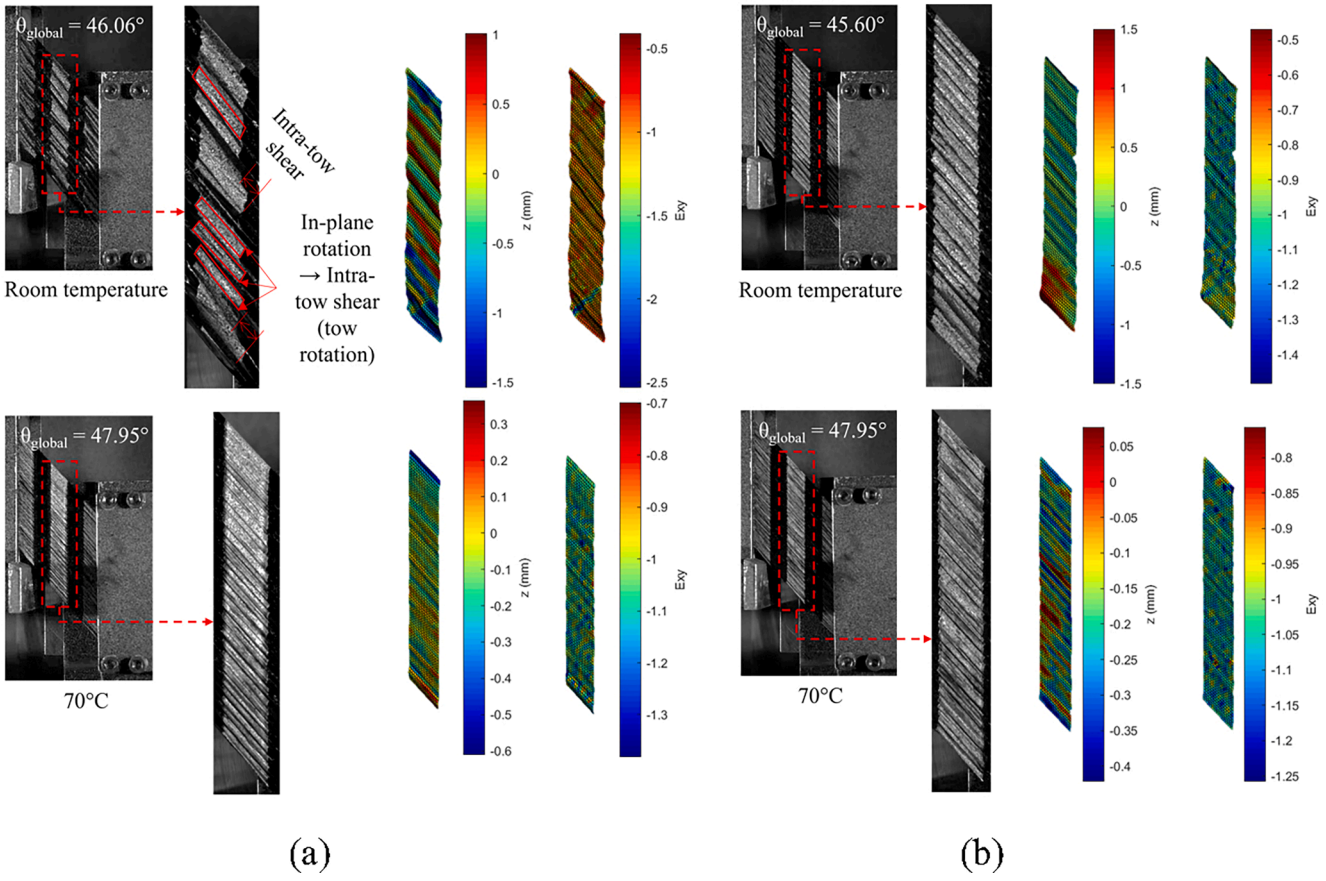

Fig. 8. Photos and DIC images of the speckled strips of (a) IM7/8552 and (b) MTM49-3/T800 specimens sheared at room temperature (left) and 70 °C (right) (shear rate: 0.01 rad/s, initial applied tension: 0.8 N/mm).

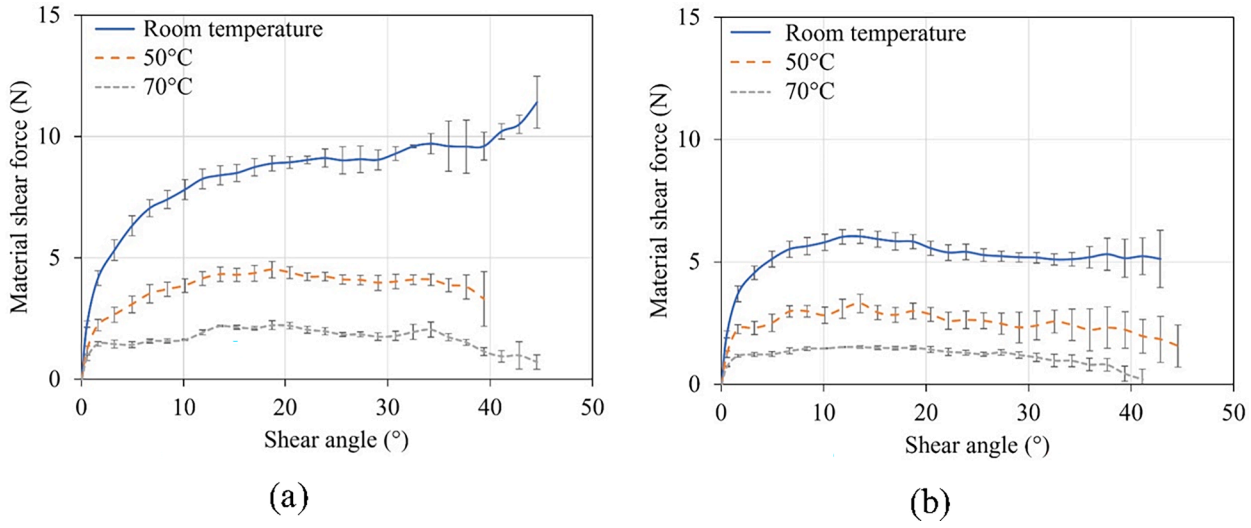

Fig. 9. Effect of temperature on the average material shear force (V_m) vs. shear angle (θ) plots of (a) IM7/8552 and (b) MTM49/T800 specimens (shear rate: 0.3 rad/s, initial applied tension: 0.8 N/mm). The error bars refer to the standard deviations.

compression [18]. Once such global wrinkles occur, transverse compressive force becomes negligible and the tension force acts along the wrinkle orientation, which is not aligned with the specimen edge [19]. For a UD tape, this can cause ply splitting and large gaps. Tow splitting (or ply splitting) also occurred due to the non-uniform distribution of the fibres and resin within the prepreg or the tows within it; the specimen was fragmented into small tows and the size of the split tow was not necessarily the same as that of the original tow used for the prepreg production. Such tow splitting was followed by tow twisting (i.e. out-of-plane rotation of the tow), due to the inherently misaligned fibres within the split tow and the lack of out-of-plane fibre movements near the clamped boundaries. These mechanisms were involved to different degrees depending on the fibre and resin distribution within the material, temperature, shear rate, and applied fibre tension level.

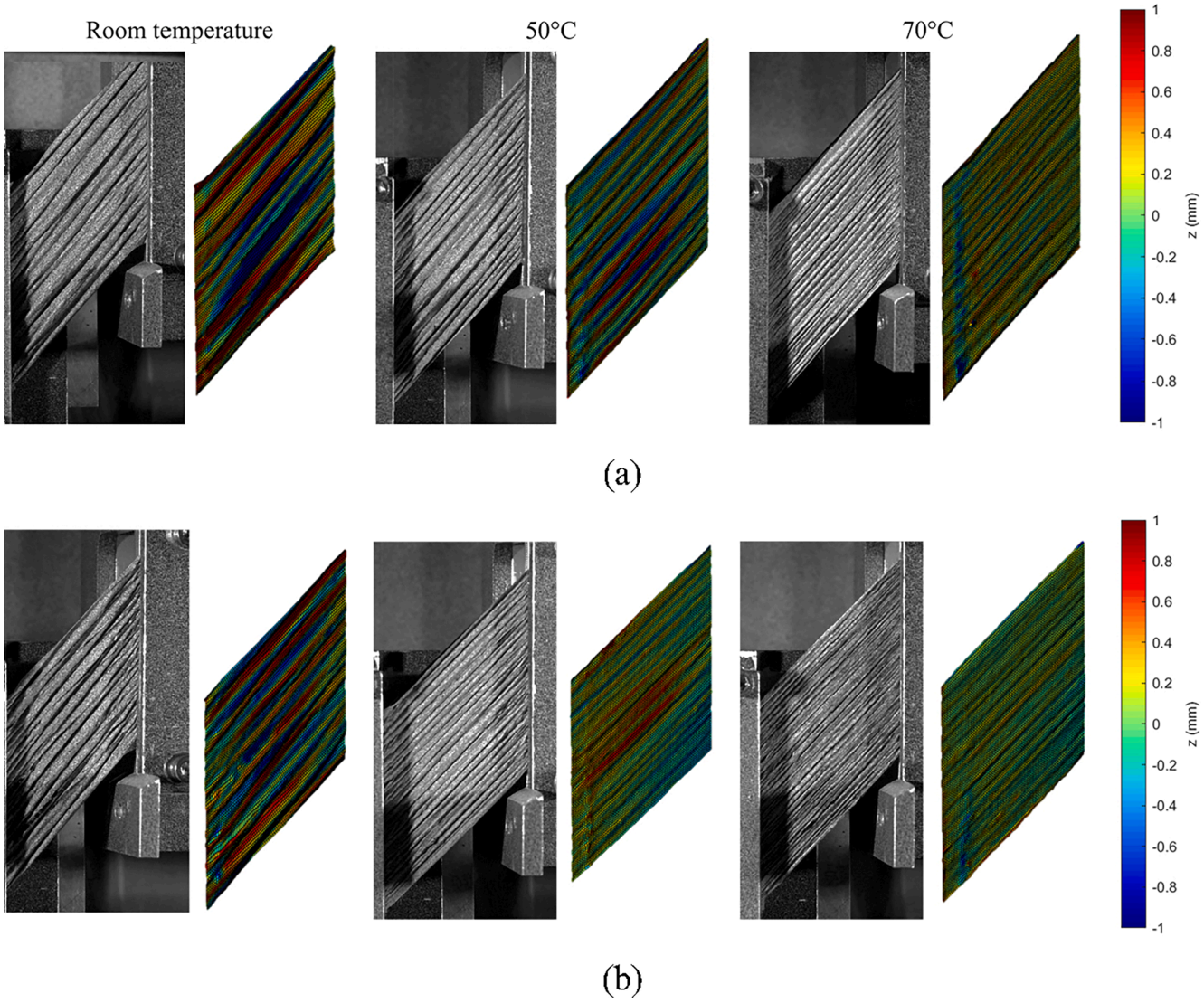

Fig. 10. Effect of temperature: photos and DIC images of (a) IM7/8552 and (b) MTM49/T800 specimens sheared at room temperature, 50 °C and 70 °C (shear rate: 0.3 rad/s, initial applied tension: 0.8 N/mm).

Consequently, a mixture of intra-tow and inter-tow shearing occurred in three dimensions rather than in the plane, which was why 3D DIC was used to capture the shear within the split and twisted tows.

Figs. 6 and 7 show the stripe-patterned sides of both prepreg specimens at different shear angles and Fig. 8 shows the magnified photos of the stripes in the middle of the specimens at the global shear angle of around 45°. Figs. 6(a) and (a) show an IM7/8552 prepreg specimen sheared at room temperature at the shear rate of 0.01 rad/s under F_w of 40 N (i.e. 0.8 N/mm × 50 mm). Global wrinkling was developed at the global shear angle of around 20°. As the global shear angle increased, the density of split tows increased. The split tows slipped relative to each other (i.e., inter-tow shearing), but without re-arranging the fibres within these tows (i.e., intra-tow shearing), and then further rotated and twisted to form rough surface and even some tow separation creating visible gaps. In contrast, when the specimen was sheared at 70 °C (see Fig. 6(b) and (b)), global wrinkling was significantly reduced, while the specimen was split into much finer tows. The overall deformation mode was close to pure intra-tow shearing. However, minimal inter-tow shearing among split tows still occurred, together with local tow twisting.

The MTM49-3/T800 specimens behaved differently from that of the IM7/8552. As shown in Figs. 7(a) and 8(b), even at room temperature, there was no significant global wrinkling. Although tow splitting and local tow twisting were observed, the split tows were much finer than the IM7/8552 specimen. The sheared surface was remarkably uniform, compared with that of the IM7/8552 specimen. As shown in Fig. 7(b), at 70 °C, the shear behaviour of the specimen was generally consistent with that of the IM7/8552 specimen due to the low resin viscosity.

It should be noted that when tow splitting and twisting occurred, DIC was not able to capture the discontinuity in the displacement field between two adjacent split tows, and the local shear angle at the discontinuity was higher than the global shear angle, which is physically impossible. Despite this limitation, the overestimated shear angle was used to indirectly assess the level of tow splitting and inter-tow shearing.

3.2. *Temperature effect*

Fig. 9 shows the average material shear force (V_m) versus the global shear angle of the specimens tested at the shear rate of 0.3 rad/s at room temperature, 50 °C and 70 °C. As temperature increased, both prepreg specimens exhibited a significant reduction in shear resistance due to the reduced resin viscosity. The shear resistance of the MTM49-3/T800 specimens was much lower than that of the IM7/8552 specimens at room temperature, which could be due to its less uniform fibre and resin

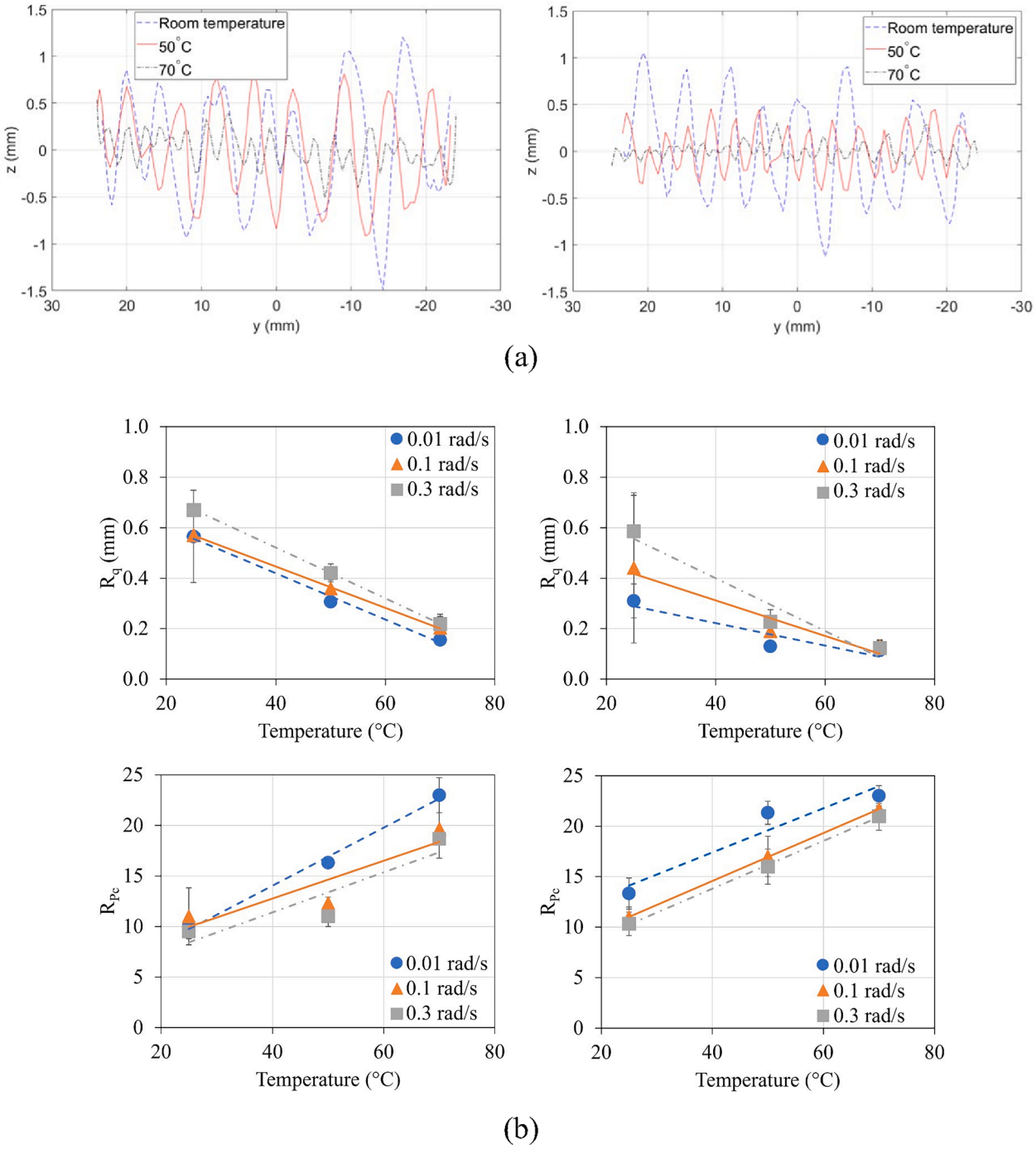

Fig. 11. Effect of temperature for IM7/8552 (left) and MTM49/T800 (right) specimens: (a) surface profiles taken at the mid-length position (shear rate: 0.3 rad/s, initial applied tension: 0.8 N/mm), and (b) average R_q and R_{Pc} values.

distribution within the tape (i.e. higher probability of tow splitting). However, the difference between both prepreg specimens was negligible at 70 °C.

Fig. 10 shows the sheared surface roughness of the specimens at the global shear angle of 46° ± 1° at room temperature, 50 °C and 70 °C. As temperature increased, the sheared surfaces of the specimens became smoother. The IM7/8552 specimens exhibited a rougher sheared surface at room temperature compared to the MTM49/T800 specimens, due to global wrinkling and less tow splitting. To assess the degree of tow splitting, surface profiles along the vertical direction at mid-length position were measured. As shown in Fig. 11(a) of the representative surface profiles, the amplitude of the peaks was consistently reduced as the temperature increased. To further investigate the results of these specimens, root-mean-square deviation (R_q) and total number of peaks (R_{Pc}) were calculated from each surface profile [21], which can reflect the degree of tow twisting and density of the split tows respectively. As shown in Fig. 11(b), the average R_q decreased, as the temperature increased from room temperature to 70 °C. The average R_{Pc} shows that for both materials, the total amount of peaks increased by a factor of 2 as temperature increased to 70 °C, which implies that the materials were better split into finer tows at high temperature.

Fig. 12(a) shows the typical local and global shear angles of both specimens at different temperatures. Each data point represents an average shear angle extracted along a vertical line crossing the centre of

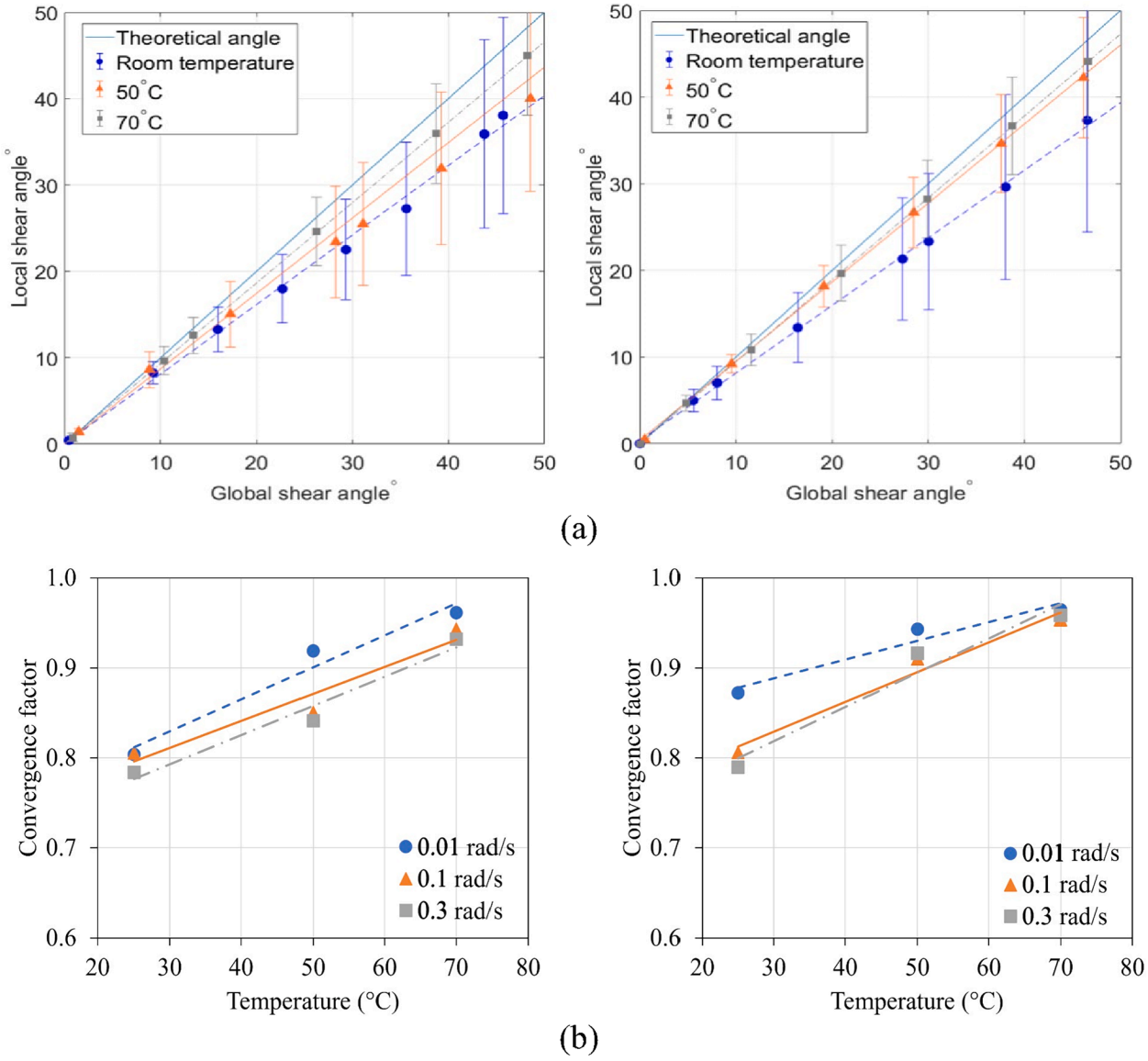

Fig. 12. Effect of temperature for IM7/8552 (left) and MTM49/T800 (right) specimens: (a) local vs. global shear angle plots (shear rate: 0.3 rad/s, initial applied tension: 0.8 N/mm), and (b) the average convergence factor vs. temperature plots.

the specimen area, while the deviation bar represents the variation of local shear angle along that line. The figure shows that at room temperature, as the global shear angle increases, the local shear angle deviates more, with the increasing shear angle variation. This implies that the level of intra-tow shearing decreases as the shear angle increases. As the temperature increased, the local shear angle became closer to the global shear angle, with the decrease of shear angle variation, which is a result of promoted intra-tow shear. At the global shear angle of 45° ± 1°, the average local shear angles of the IM7/8552 and MTM49/T800 specimens were 7.7° and 9.2° away from the measured global shear angle at room temperature, and only within 2° difference at 70 °C. Also, the deviation of the local shear angle of both prepreg specimens reduced by up to 50% when the temperature increased from room temperature to 70 °C.

To show the temperature effect more concisely, linear regression was used to derive the convergence factor, which is the ratio of average local shear angle to global shear angle that reflects the degree of intra-tow shear or the uniformity of the shear deformation. They were averaged and plotted versus temperature in Fig. 12(b). It can be seen that as the temperature increased, the factor became closer to 1, indicating that the material was sheared more uniformly.

3.3. Shear rate effect

Fig. 13 shows the average material shear force (V_m) versus global shear angle plots of both prepreg specimens tested at the shear rates of 0.01, 0.1 and 0.3 rad/s at room temperature. It shows that both prepregs exhibited higher shear resistance with increase of shear rate, due to the viscoelastic behaviour of the resin matrix. Also, even though the matrix viscosity of both prepregs was similar, there was some differences at room temperature, which is potentially due to their different void and resin distributions (discussed in Section 2.1). However, at 70 °C, both prepreg specimens exhibited almost the same behaviour, as the viscosity of both resin systems became very low.

Fig. 14 shows the sheared surfaces extracted from the 3D DIC at room temperature. As the shear rate increased, greater tendency of global wrinkling followed by tow splitting and twisting were observed, while the MTM49-3/T800 specimens exhibited relatively smoother surfaces. However, at 70 °C, there was no apparent difference, therefore the results are not presented. The trend described above is summarised in

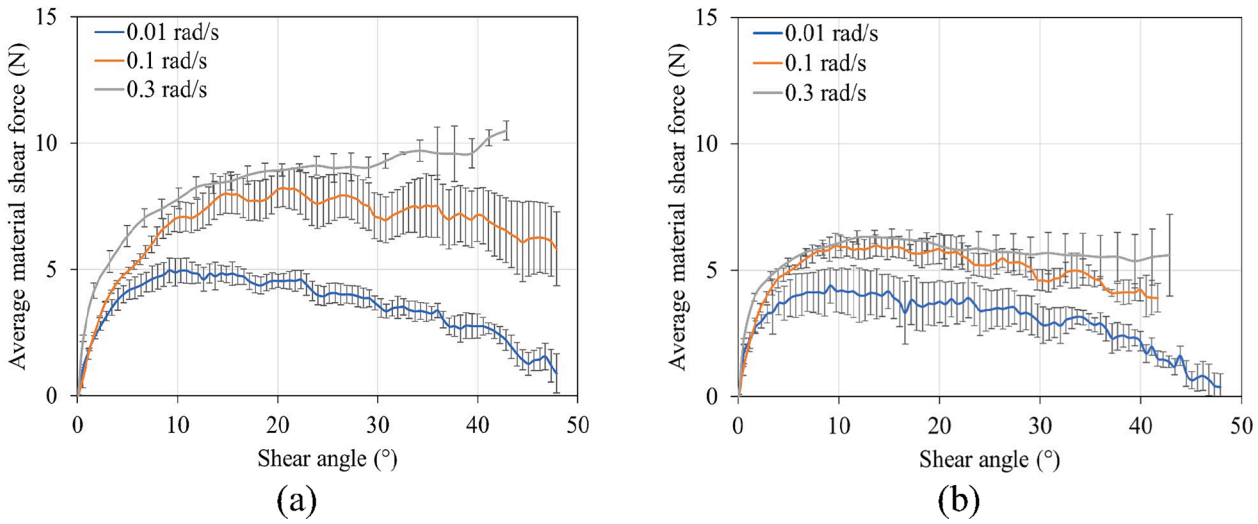

Fig. 13. Effect of shear rate at room temperature: average material shear force (V_m) vs. shear angle (θ) plots of (a) IM7/8552 and (b) MTM49/T800 specimens (initial applied tension: 0.8 N/mm). The error bars refer to the standard deviations.

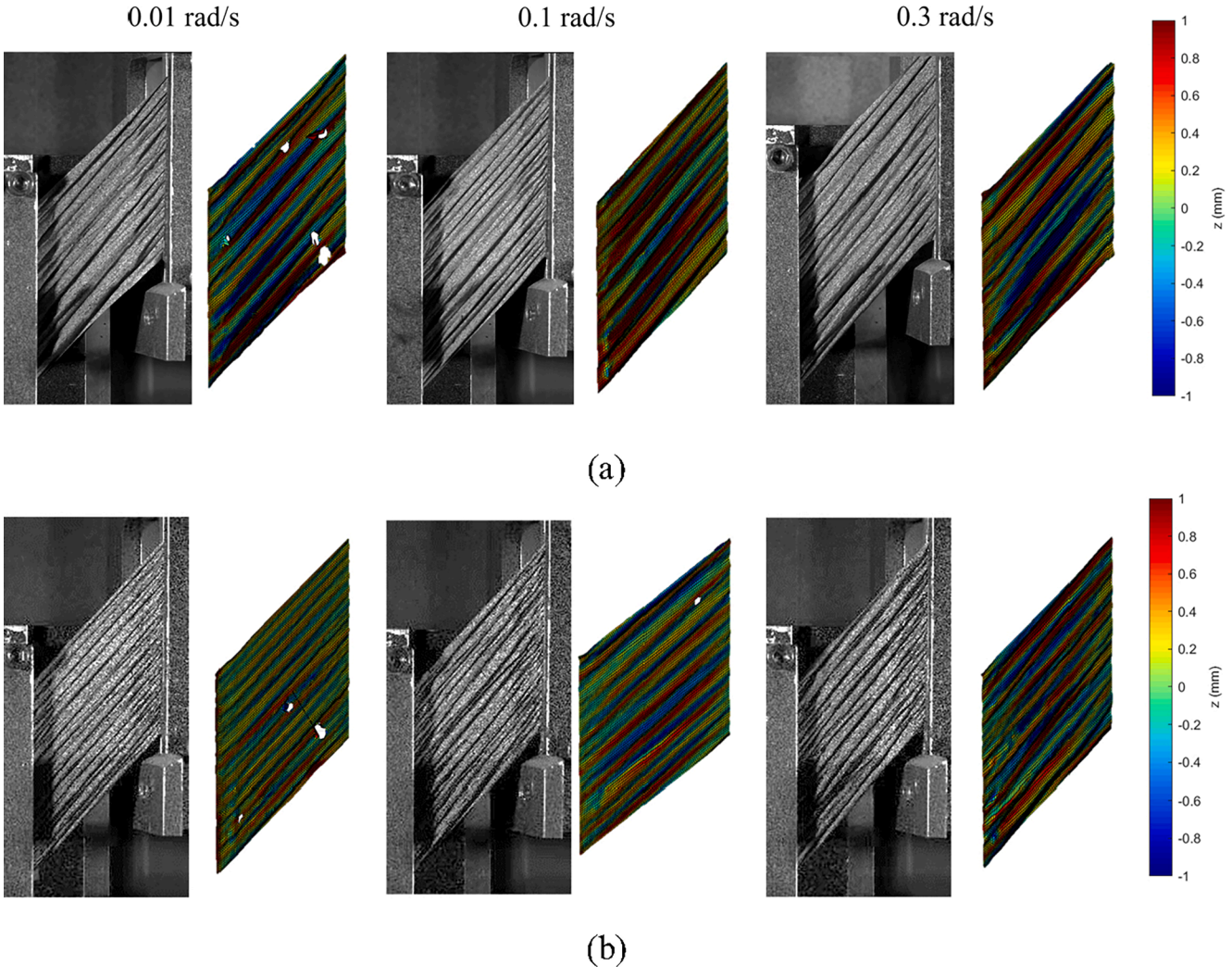

Fig. 14. Effect of shear rate at room temperature: photos and DIC images of (a) IM7/8552 and (b) MTM49/T800 specimens (initial applied tension: 0.8 N/mm).

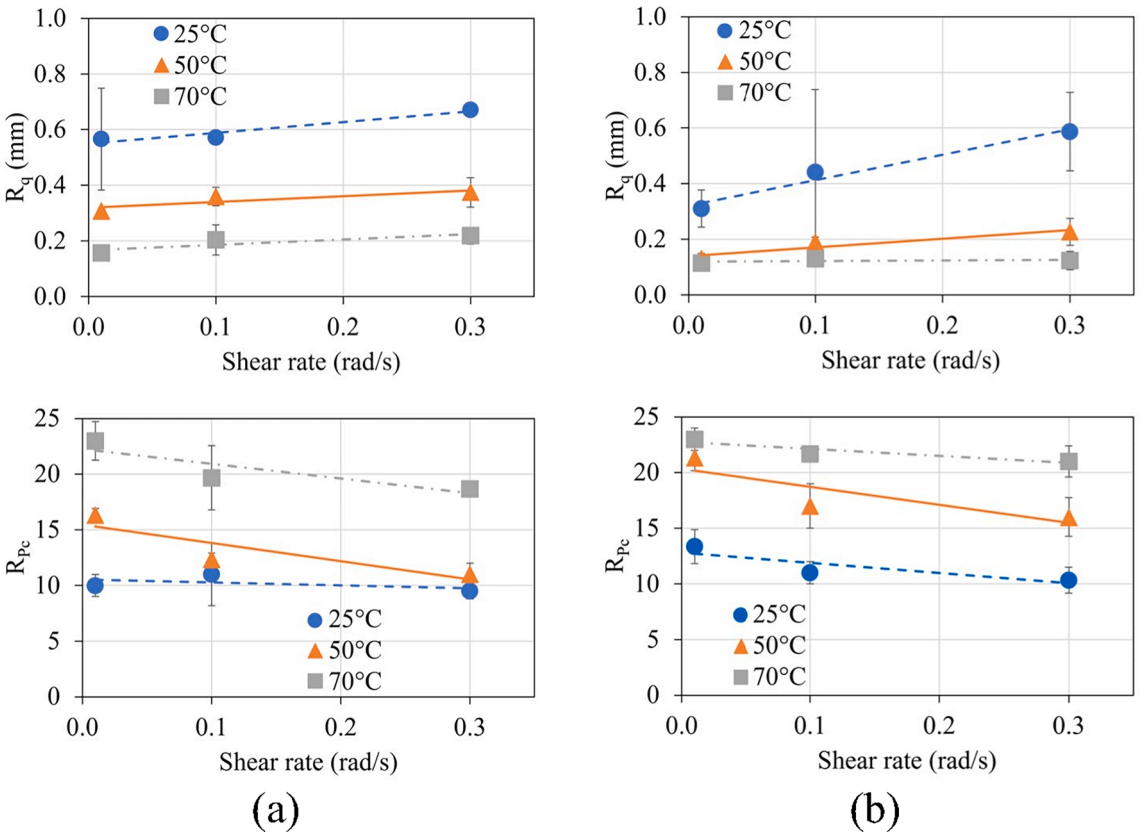

Fig. 15. Effect of shear rate: average R_q and R_{Pc} vs. shear rate plots of (a) IM7/8552 and (b) MTM49/T800 specimens (initial applied tension: 0.8 N/mm).

Fig. 15 plotting the average R_q and R_{Pc} values at different shear rates. The R_q values of both prepreg specimens increased with increasing shear rate at room temperature, while those of the MTM49-3/T800 specimens were smaller in general. The R_{Pc} values showed that the total amount of peaks reduced with increase of shear rate, indicating that the specimens split into large tows at high shear rate and thus greater out-of-plane tow twisting occurred.

Fig. 16(a) shows the shear angle plots of both prepreg specimens at different shear rates at room temperature. For both prepreg specimens, the maximum average local shear angle was around 5° away from the measured global shear angle of 45° ± 1° at the shear rate of 0.01 rad/s, and was more than 8° and 10° respectively at the shear rate of 0.3 rad/s. Also, the standard deviation increased remarkably with shear rate. At 70 °C, the average local shear angles of both prepreg specimens were very close to the measured global shear angle (within 2° difference). Fig. 16(b) plots the average convergence factors derived from the average local shear angles as a function of shear rate. The average convergence factors decreased as the shear rate increased. At 70 °C, the slopes were almost constant regardless of shear rate.

3.4. Tension level effect

Fig. 17 shows the average material shear force versus shear angle plots at various applied fibre tension levels at 70 °C. Regardless of the applied fibre tension, both prepreg specimens exhibited similar shear resistances. Although the high fibre tension was able to constrain the out-of-plane movement of the fibres, the shear resistance was not affected, potentially due to the lubrication effect of the resin matrix. The shear tests were conducted only at the highest applied tension level of 0.8 N/mm at room temperature, as tow splitting and twisting, and tow separation were too obvious on both prepreg specimens at lower applied tension levels.

Fig. 18 shows the sheared specimens at the maximum shear angle at the applied fibre tension of 0.2, 0.4 and 0.8 N/mm at 50 °C and 70 °C. At low applied tension levels, the fibres were more capable of moving out of the plane, causing tow splitting and twisting. Whereas at high applied tension levels, the specimens were split into finer tows, which resulted in a smoother specimen surface. Fig. 19 plots the average R_q and R_{Pc} values of the specimens at different tension levels. As the applied fibre tension increased, the average R_q decreased, where the average R_q decreased by 55.8% and 58.9% respectively at high applied fibre tensions of 0.8 N/mm at 50 °C and 70 °C cases. It also shows that the average R_{Pc} of both prepreg specimens increased with increase of fibre tension, indicating that finer split tows were formed.

Fig. 20(a) shows the shear angle plots at various applied tension levels at 50 °C and 70 °C. At 50 °C, the maximum average local shear angle of the IM7/8552 and MTM49/T800 specimens were around 10° and 8° away from the measured global shear angle at the applied tension level of 0.2 N/mm, and was within 8° and 5° respectively at the applied tension level of 0.8 N/mm. Low fibre tension resulted in inter-tow shearing due to significant tow splitting and twisting, whereas high fibre tension resulted in a higher local shear angle close to the global shear angle. The standard deviation was greatly reduced with increase of applied tension level, which is attributed to the formation of finer split tows minimising out-of-plane twisting. At 70 °C, the average local shear angles became even more close to the global shear angle as the applied fibre tension increased. The deviation of the local shear angle from the global shear angle of the IM7/8552 and MTM49/T800 specimens was reduced by over 50% compared with their 50 °C cases, due to the decreased resin viscosity. Fig. 20(b) shows the convergence factor derived from the average local shear angle results as a function of the applied tension at 50 °C and 70 °C. It can be seen that the convergence factor of both prepreg materials increased with applied tension level.

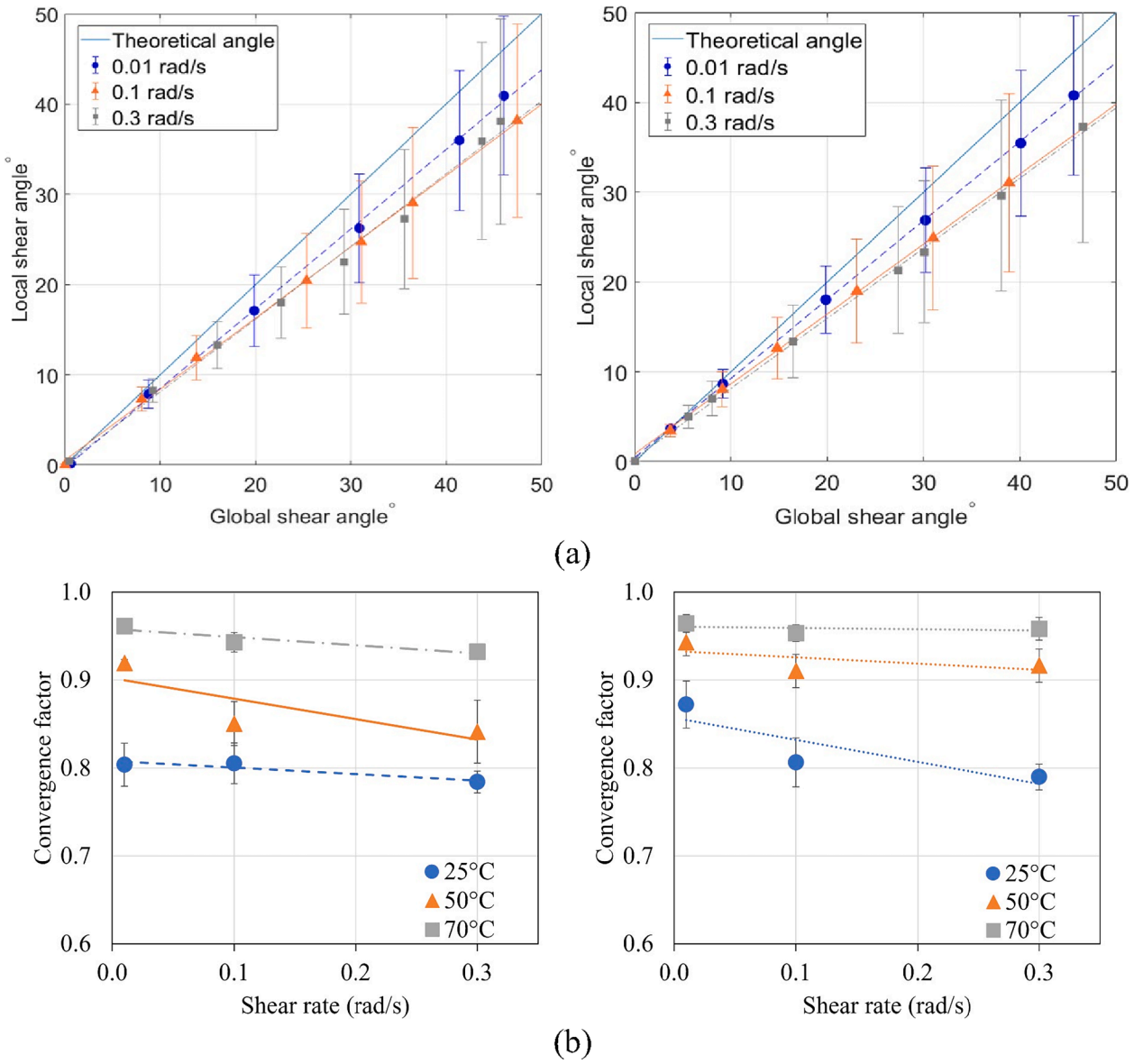

Fig. 16. Effect of shear rate for IM7/8552 (left) and MTM49/T800 (right) specimens: (a) local shear angle vs. global shear angle plots at various shear rates at room temperature and (b) average convergence factor vs. shear rate plots (initial applied tension: 0.8 N/mm).

4. Discussion

The experimental results showed that the processing conditions significantly affect the levels of inter-tow shearing between split tows and intra-tow shearing within the split tows as well as the density of tow splitting and degree of tow twisting. In the CTS process, it is of importance to achieve a high degree of intra-tow shear to minimise the defect formation. However, the effect of the inter-tow shearing on fibre-steering process-induced defects was not explicitly demonstrated in this experiment, as the shearing angle was constant in the specimens. In the fibre steering using the CTS process with continuously varying shearing angle, it is clear that more inter-tow shearing will result in more in-plane bending-induced wrinkles, but the level of such wrinkles would still be considerably smaller than those formed in the AFP processes.

The effect of processing temperature on promoting the intra-tow shearing was clearly observed. At low temperature, high matrix viscosity limited the fibre rearrangements, making the tape prone to buckling in shear at the beginning and then splitting into wide tows. The split tows were twisted in the out-of-plane direction, but not sheared. However, at elevated temperature, low matrix viscosity allowed the fibres to be realigned more easily without global wrinkling, which was more close to pure intra-tow shearing and significantly decreased the material shear resistance. The specimen was split into much narrower tows due to the inhomogeneity within the material and the inherent fibre misalignment, causing some inter-tow shearing. This temperature effects on the tow band/split tow formation and on the shear force reduction were consistent with the observations from the previous bias extension and 10° off-axis tension tests [14,15].

The shear rates affected the shear performance of the tapes, but only at low temperature. At low temperature and high shear rate, significant global wrinkling and twisting of wide split tows were observed, but as shear rate decreased, such behaviour became less. Whereas at high temperature, the viscoelastic effect became almost negligible, and so upon shearing this resulted in more uniformly sheared specimen surfaces with high degree of intra-tow shearing, even at high shear rate. This was also observed by Larberg et al. [14] from their bias extension test that depending on applied crosshead speeds, prepregs were divided into split tows and then inter-tow shear or slip was observed. The increase of the material shear force of both prepregs with the shear rates

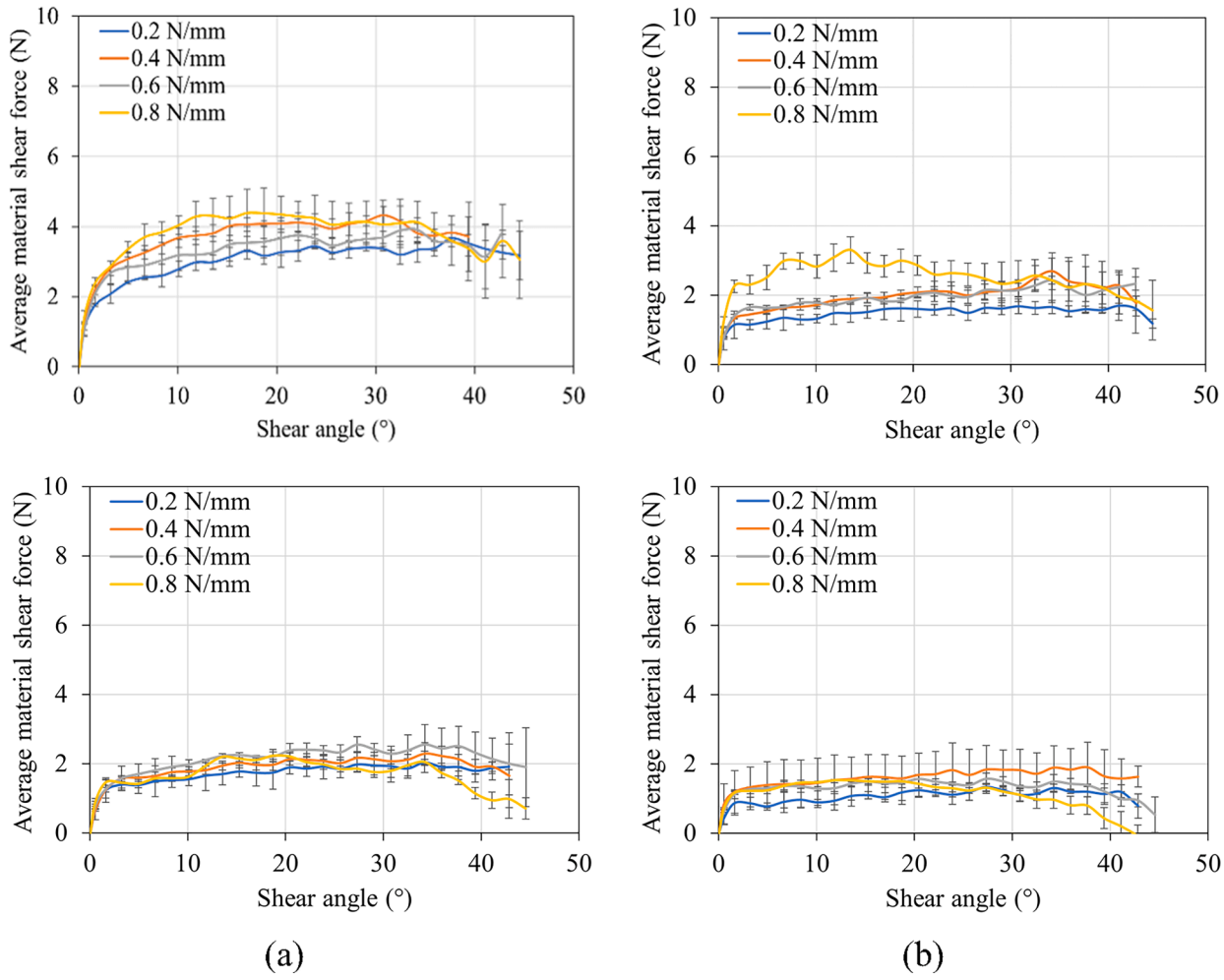

Fig. 17. Effect of applied fibre tension: average material shear force (V_m) vs. shear angle (θ) at different initial tensions for (a) IM7/8552 and (b) MTM49/T800 specimens at 50 °C (top) and 70 °C (bottom) (shear rate: 0.3 rad/s). The error bars refer to the standard deviations.

was consistent with the results from bias-extension test [13] and from 10° off-axis tension tests [15].

In addition, the effect of applied fibre tension on the intra-tow shearing was significant. In-plane shearing of a UD prepreg tape with fixed boundaries causes not only the in-plane fibre rearrangement, but also out-of-plane fibre rearrangement causing transverse compaction (with closure of internal voids and potentially resin squeeze-out particularly at high shear angle) which resulted in the thickness change. The fibre tension was very effective to constrain the out-of-plane movement of the fibres and make them follow the global shear angle. With low fibre tension, global wrinkling promoted coarse tow splitting and inter-tow shearing of the split tows. As the fibre tension increased, the density of tow splitting was significantly increased, while the wrinkle orientation was more aligned with the global shear angle direction.

It was also found that the impregnation characteristic of the prepregs influenced the shear behaviour, particularly at room temperature. Fig. 21 shows the cross-sectional micrographs of the specimens shown in Fig. 8; since the microscopy specimens were prepared after taking out the specimens from the test rig and cured at room temperature for a long time, there was some relaxation of the deformation due to the absence of shearing and tension forces. At room temperature, as shown in Fig. 21 (a), the IM7/8552 specimen maintained its fibre integrity well during shearing and was prone to global wrinkling with a few large splits. This global wrinkling could lead to defects when the surface is compressed by a compaction shoe in the CTS process, as the wrinkling orientation is not well aligned to the global shear angle. In comparison, the inhomogeneity within the MTM49-3/T800 specimen (i.e. less uniform fibre and resin distributions and randomly distributed voids) seemed to make the specimen more susceptible to tow splitting and even folding under the transverse compression during shearing, which resulted in a lower surface roughness and a better overall fibre rearrangement. At 70 °C, as shown in Fig. 21(b), the effect of material inhomogeneity became minor due to the decreased resin viscosity, although the cross-section of the MTM49-3/T800 specimen exhibited slightly more folding and splitting.

5. Conclusions

In this work, the effect of processing parameters in the CTS process, such as temperature, shear rate and fibre tension, on the shear behaviour of unidirectional carbon fibre/epoxy prepreg tapes subjected to large shear deformation was investigated using a bespoke test fixture. The bespoke test fixture with the use of digital image correlation technique was able to assess the uniformity of shearing of UD prepreg tapes under the shearing conditions of the CTS process by comparing the local shear angle distribution with the global shear angle, and to measure the surface roughness parameters which reflected the degree of inter-tow and intra-tow shearing, tow splitting and twisting.

The test results showed that both temperature and fibre tension are critical to the fibre realignment during shearing, whereas the shear rate effect is almost negligible when the temperature is sufficiently high due

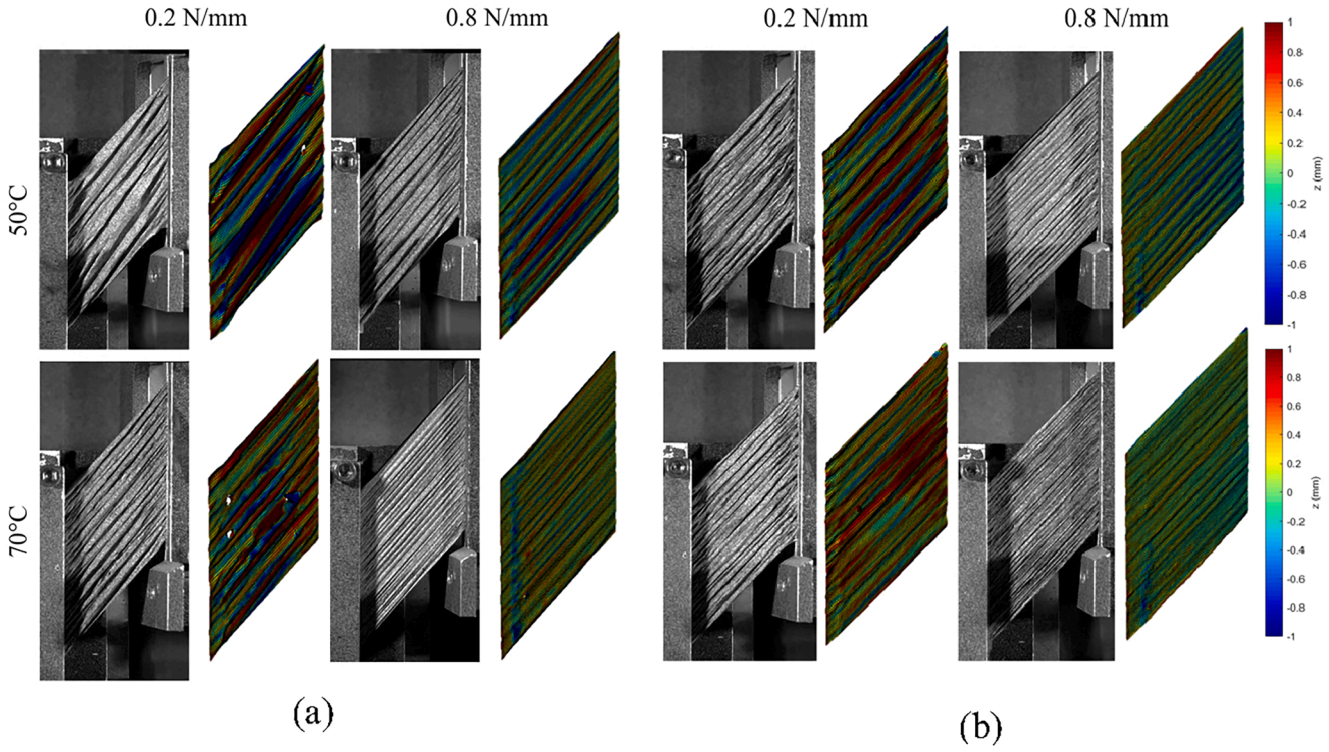

Fig. 18. Effect of applied fibre tension: photos and DIC images of (a) IM7/8552 and (b) MTM49/T800 specimens sheared at initial fibre tension of 0.2 and 0.8 N/mm at 50 °C and 70 °C (shear rate: 0.3 rad/s).

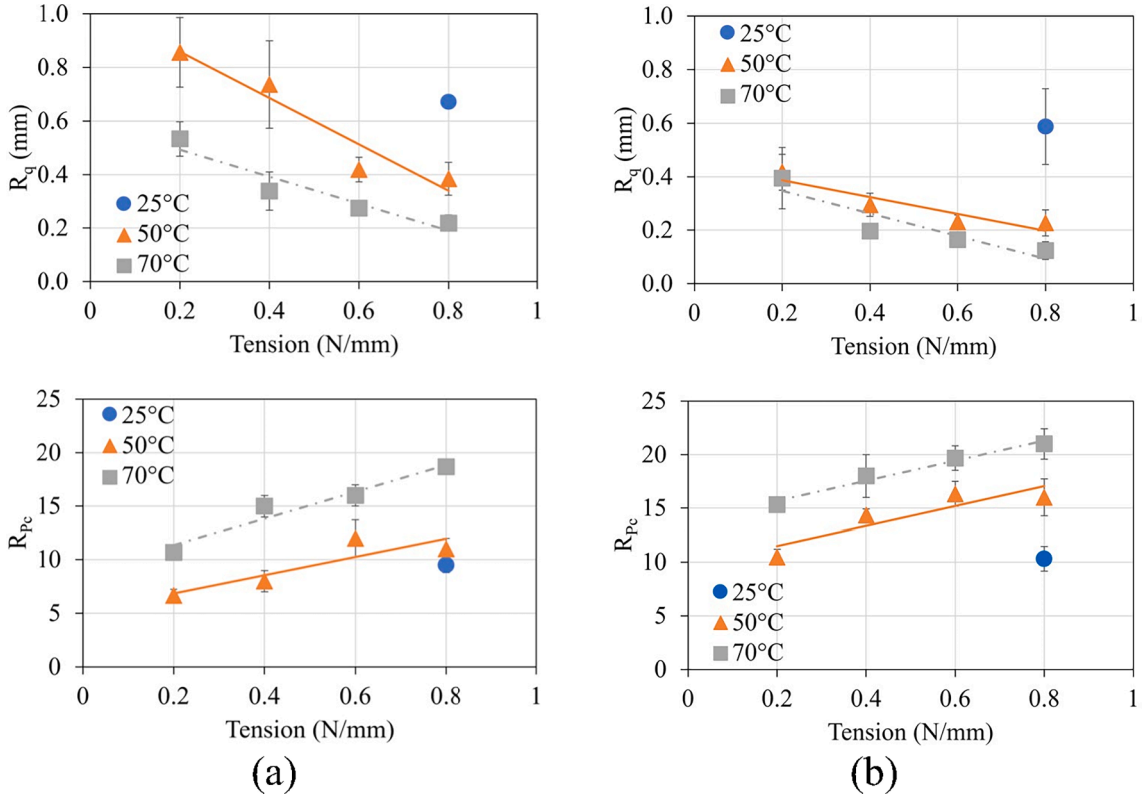

Fig. 19. Effect of applied fibre tension: average R_q and R_{Pc} as a function of initial applied tension for (a) IM7/8552 and (b) MTM49/T800 specimens (shear rate: 0.3 rad/s).

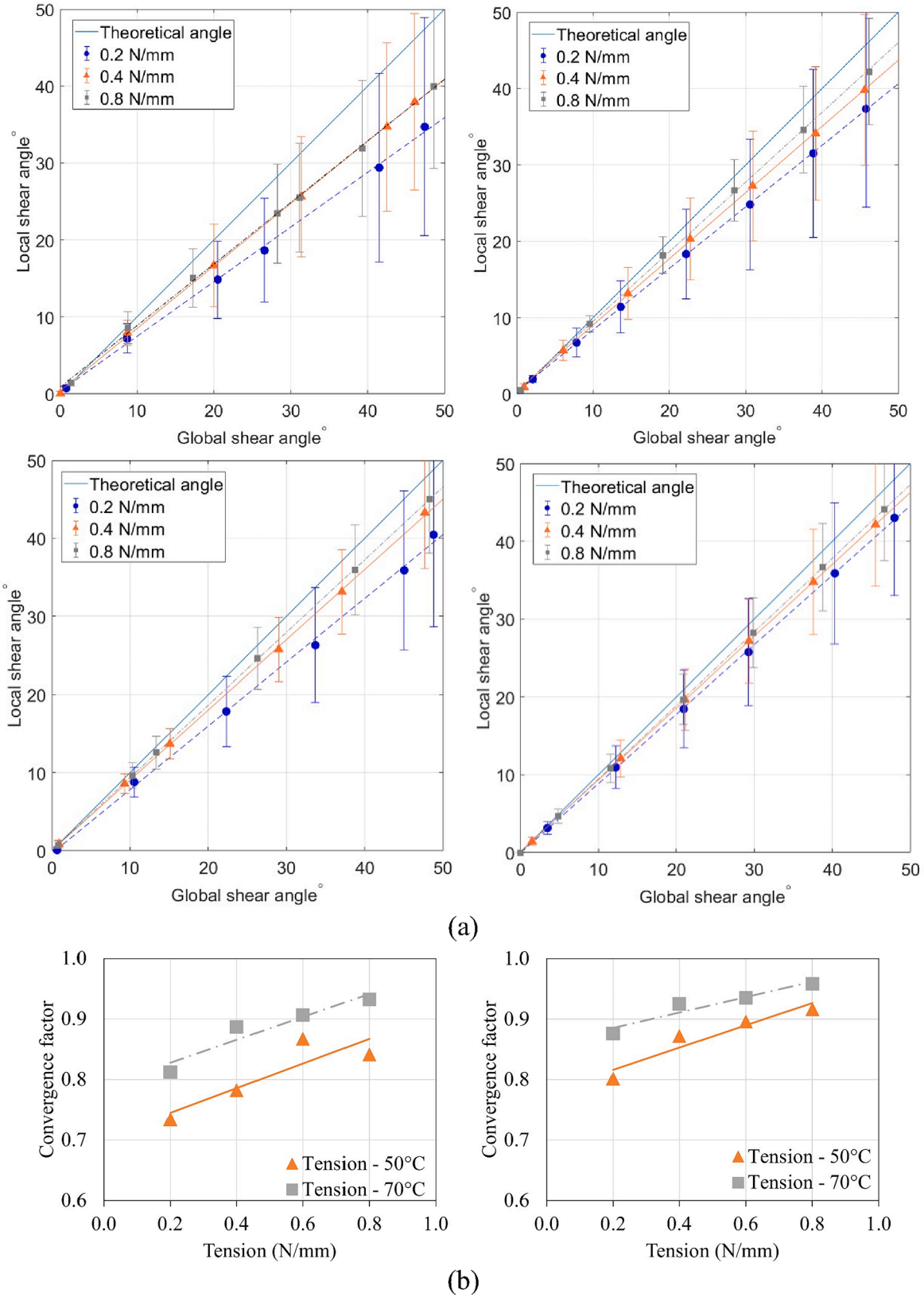

Fig. 20. Effect of applied tension for IM7/8552 (left) and MTM49/T800 (right) specimens: (a) local–global shear angle plots at different applied tensions at 50 °C (top) and 70 °C (bottom) and (b) average convergence factor vs. applied tension plots at 50 °C and 70 °C (shear rate: 0.3 rad/s).

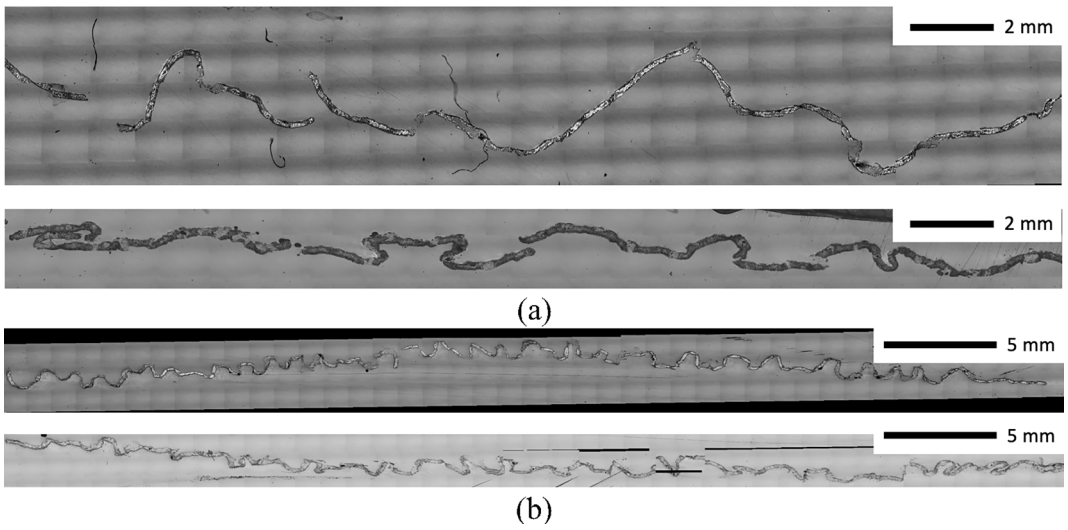

Fig. 21. Cross-sections of the IM7/8552 (upper) and MTM49-3/T800 (lower) specimens sheared: (a) at room temperature and (b) at 70 °C (shear rate: 0.01 rad/s, initial applied tension: 0.8 N/mm).

to the reduction of the resin viscosity (1600 Pa·s, and 250 Pa·s at 50 °C and 70 °C respectively). Low viscosity of the resin matrix was important to allow the fibre realignment and thus to achieve more uniform inter-tow shearing. High fibre tension allowed fibres to maintain the straightness when transverse compaction was induced, while increasing the density of tow splitting. For the CTS process, an optimal processing temperature should be firstly determined. However, its impact on the tackiness of the resin for deposition and adhesion between the prepreg tape and the backing paper should be considered. A high fibre tension could be good, but it requires a more robust structure of the deposition head. This could lead to increase the weight and cost of the equipment.

In addition to the process parameters, the impregnation characteristic and inherent fibre misalignment within the prepreg tapes were important. It was difficult to quantitatively investigate these in this study, but the shear buckling (out-of-plane movement) and split tow density at room temperature could indirectly assess them.

CRediT authorship contribution statement

Bohao Zhang: Conceptualization, Methodology, Validation, Investigation, Data curation, Writing – original draft, Writing – review & editing. **Byung Chul Kim:** Conceptualization, Methodology, Writing – review & editing, Supervision, Project administration, Funding acquisition.

Declaration of Competing Interest

The authors declare that they have no known competing financial interests or personal relationships that could have appeared to influence the work reported in this paper.

Acknowledgement

This work was funded by the EPSRC project “Advanced Continuous Tow Shearing in 3D (ACTS3D): Advanced fibre placement technology for manufacturing defect-free complex 3D composite structures” (EP/R023247/1). All data required for reproducibility is included in the paper.

References

[1] Dirk H-J-L, Ward C, Potter KD. The engineering aspects of automated prepreg layup: History, present and future. Compos B Eng 2012;43(3):997–1009.
[2] Croft K, Lessard L, Pasini D, Hojjati M, Chen J, Yousefpour A. Experimental study of the effect of automated fiber placement induced defects on performance of composite laminates. Compos A Appl Sci Manuf 2011;42(5):484–91.
[3] Potter K, Langer C, Hodgkiss B, Lamb S. Sources of variability in uncured aerospace grade unidirectional carbon fibre epoxy preimpregnate. Compos A Appl Sci Manuf 2007;38(3):905–16.
[4] Matveev MY, Schubel PJ, Long AC, Jones I. Understanding the buckling behaviour of steered tows in Automated Dry Fibre Placement (ADFP). Compos A Appl Sci Manuf 2016;90:451–6.
[5] Kim BC, Potter K, Weaver PM. Continuous tow shearing for manufacturing variable angle tow composites. Compos A Appl Sci Manuf 2012;43(8):1347–56.
[6] Kim BC, Weaver PM, Potter K. Manufacturing characteristics of the continuous tow shearing method for manufacturing of variable angle tow composites. Compos A Appl Sci Manuf 2014;61:141–51.
[7] Zympeloudis E, Potter K, Weaver PM, Kim BC. Advanced automated tape laying with fibre steering capability using continuous tow shearing mechanism. 21st international conference on composites materials. 2017.
[8] Cao J, Akkerman R, Boisse P, Chen J, Cheng HS, de Graaf EF, et al. Characterization of mechanical behavior of woven fabrics: experimental methods and benchmark results. Compos A Appl Sci Manuf 2008;39(6):1037–53.
[9] Harrison P, Clifford MJ, Long A. Shear characterisation of viscous woven textile composites: a comparison between picture frame and bias extension experiments. Compos Sci Technol 2004;64(10–11):1453–65.
[10] Gereke T, Döbrich O, Hübner M, Cherif C. Experimental and computational composite textile reinforcement forming: a review. Compos A Appl Sci Manuf 2013;46:1–10.
[11] Boisse P, Hamila N, Guzman-Maldonado E, Madeo A, Hivet G, Dell'Isola F. The bias-extension test for the analysis of in-plane shear properties of textile composite reinforcements and prepregs: a review. Int J Mater Form 2017;10(4):473–92.
[12] McGuinness G, ÓBrádaigh C.. Characterisation of thermoplastic composite melts in rhombus-shear: the picture-frame experiment. Compos A Appl Sci Manuf 1998;29(1–2):115–32.
[13] Potter K. Bias extension measurements on cross-plied unidirectional prepreg. Compos A Appl Sci Manuf 2002;33(1):63–73.
[14] Larberg YR, Åkermo M, Norrby M. On the in-plane deformability of cross-plied unidirectional prepreg. J Compos Mater 2012;46(8):929–39.
[15] Wang Yi, Chea MK, Belnoue J-H, Kratz J, Ivanov DS, Hallett SR. Experimental characterisation of the in-plane shear behaviour of UD thermoset prepregs under processing conditions. Compos A Appl Sci Manuf 2020;133:105865.
[16] HexPly 8552 – Material properties database for use with COMPRO CCA and Raven; 15th Nov 2009. <https://www.wichita.edu/industry_and_defense/NIAR/Research/hexcel-8552/Additional-Documents-2.pdf>.
[17] Harrison P, Abdiwi F, Guo Z, Potluri P, Yu W. Characterising the shear–tension coupling and wrinkling behaviour of woven engineering fabrics. Compos A Appl Sci Manuf 2012;43(6):903–14.
[18] Wong W, Pellegrino S. Wrinkled membranes I: experiments. J Mech Mater Struct 2006;1(1):3–25.
[19] Iwasa T. Approximate estimation of wrinkle wavelength and maximum amplitude using a tension-field solution. Int J Solids Struct 2017;121:201–11.
[20] Harrison P, Clifford M, Long A, Rudd C. A constituent-based predictive approach to modelling the rheology of viscous textile composites. Compos A Appl Sci Manuf 2004;35(7–8):915–31.
[21] Gadelmawla E, Koura MM, Maksoud TM, Elewa IM, Soliman H. Roughness parameters. J Mater Process Technol 2002;123(1):133–45.